Journal of Marine Science and Technology

Volume 30 | Issue 2 Article 4

Sensitive Analysis of the Static Response of Compliant Vertical Access Risers

Fuheng Li
College of Engineering, Ocean University of China, Qingdao, 266100, China

Haiyan Guo
College of Engineering, Ocean University of China, Qingdao, 266100, China, hyguo@ouc.edu.cn

Xiaomin Li
College of Engineering, Ocean University of China, Qingdao, 266100, China

Honglu Gu
College of Engineering, Ocean University of China, Qingdao, 266100, China

Recommended Citation

Li, Fuheng; Guo, Haiyan; Li, Xiaomin; and Gu, Honglu (2022) "Sensitive Analysis of the Static Response of Compliant Vertical Access Risers," *Journal of Marine Science and Technology*: Vol. 30: Iss. 2, Article 4.
DOI: 10.51400/2709-6998.2571
Available at: https://jmstt.ntou.edu.tw/journal/vol30/iss2/4

RESEARCH ARTICLE

Sensitive Analysis of the Static Response of Compliant Vertical Access Risers

Fuheng Li, Haiyan Guo*, Xiaomin Li, Honglu Gu

College of Engineering, Ocean University of China, Qingdao, 266100, China

Abstract:

Compliant vertical access risers (CVARs) are considered as efficient and robust alternative options to achieve cost efficiency and safety. Design uncertainties emerge owing to the limited understanding of the effects of various parameters related to the structural properties and marine loads. In this paper, a reasonable three-dimensional (3D) numerical model of CVAR with internal flow is presented based on the slender rod theory. Accordingly, the finite element method combined with a Newton−Raphson scheme is employed to discretize and solve equations. A sensitivity analysis is performed to investigate the influence of the structural and external load parameters on the static behavior of the CVAR. The effects of the weight and length of the respective functional segments with unchanged wet weight are analyzed and compared. The results indicate that the lengths of the buoyancy and weight segments affect not only the bending moment extremums and effective tension of the CVAR but also the extremum locations of the bending moment. Moreover, an increase in the weight per unit length of these segments leads to an increase in the bending moment extremums of the CVAR. The overall deformation of the CVAR is sensitive to current velocity along the y-direction. However, large tension and bending moment responses are easily provoked by the current velocity along the x-direction. This is also true for the tension and bending moment in the riser induced by the vessel motion along the x-direction.

Keywords: Compliant vertical access riser, Slender rod theory, Sensitive analysis, Structural parameters, Marine loads

1. Introduction

Offshore risers are usually of the following types: top tensioned risers (TTRs), flexible risers (FRs), hybrid risers (HRs), and steel catenary risers (SCRs). However, as energy exploration and production extend to increasingly deeper waters, TTRs will no longer be applicable, and FRs are incapable of high temperature and pressure fields due to their manufacturing technique [2]. HRs are vulnerable to severe fatigue damage at the connection joints from towing to installation [23], and SCRs present high hang-off tension levels as the suspended length increases [21]. Furthermore, higher cost and larger fluid forces induced by long buoyancy modules are issues encountered with steel lazy wave risers (SLWRs) in deep waters [25]. Hence, a new form of riser is urgently required.

The concept of CVAR was first proposed by [19]; as shown in Fig. 1. It is a lower-tension compliant riser for production activities in deep and ultra-deep waters that characterized by its differentiated geometry, which is attributed to a buoyancy module at the lower parts of the riser and an additional weight segment in its upper region [16]. A critical feature is that the transition region results in a substantial riser motion decoupling between the top and lower parts. Moreover, the almost vertical configuration state of both ends under this type of arrangement contributes to the fatigue life. More importantly, CVAR systems allow direct intervention procedures to the well head, and the workover can be

Received 24 August 2021; revised 6 October 2021; accepted 16 March 2022.
Available online 17 May 2022.

* Corresponding author.
E-mail address: hyguo@ouc.edu.cn (H. Guo).

https://doi.org/10.514/2709-6998.2571

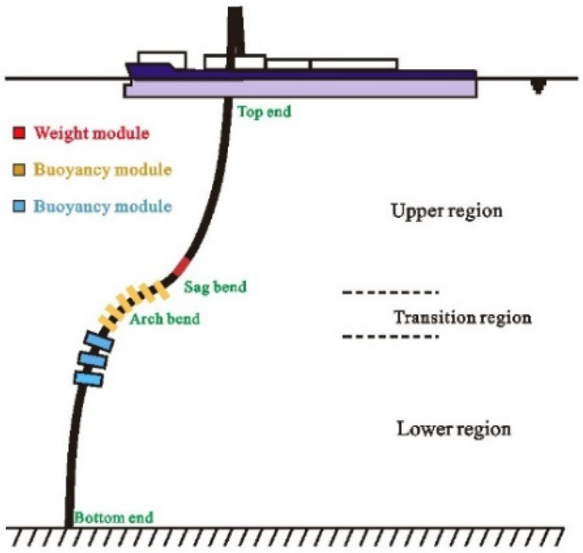

Fig. 1. Schematic of a CVAR [15].

performed from the production platform without hiring specific units, which means that these systems are economically desirable. Thus, a novel CVAR configuration riser can be regarded as a reliable, robust, and reasonable selection that takes cost savings and safety risk into consideration.

[1] used Flexcom-3D to analyze the dynamic response and fatigue life of CVAR under top-end motion [6]. used a commercial software to investigate the VIV damage and vessel-induced extreme response of CVAR. Although accurate results of the numerical simulation can be obtained by using commercial software, such as OrcaFlex, Flexcom-3D, and Riflex, it is time-consuming to establish a numerical model and process the results using a cumbersome graphical user interface. Generally, these software programs are employed in the final stage of riser design for accurate results [11,15]). Engineers tend to use convenient simulation methods for the intermediate stages of riser design to quickly adjust the riser parameters [27]. utilized the design of experiment (DOE) method to establish an approximate model, and performed simple weight optimization for CVAR [16,17]. studied the optimal solution of the CVAR dynamic response under top-end motion using the same method. However, the effects of the structural parameters require further study [13−15]. used virtual work and variational principles to perform a relatively comprehensive analysis of the structural optimization, static response, and dynamic response of the CVAR. However, only a simple static analysis of the effect of the buoyancy module parameters in the transition region was performed, and the influences of other parameters, such as the buoyancy module in the lower region and the weight segment in the upper region, were neglected. Therefore, it can be concluded from the above literature review that there is a lack of systematic study of CVAR, particularly for its static analysis, which seriously restricts the progress of design and application. Thus, sensitivity analyses should be performed to examine the influence of structural parameters, and the differences in the effects of the buoyancy factor (weight factor) and length of functional segments need to be clarified. An understanding of the CVAR response should also be facilitated when subjected to ocean current and vessel offsets.

This study investigates the effects of structural and load parameters on the static behavior of a CVAR. Critical innovation emphasizes the comparison between the length and the factor of the functional segments, which is different from other literature with respect to parameter sensitivity analysis. The numerical scheme of CVAR is proposed by the slender rod theory, which describes the behavior of risers in terms of the centerline position [9,18]. The key benefit is that the geometrical nonlinearity of CVAR can be solved effectively, and the calculation efficiency is improved by avoiding the tedious process of the traditional finite element method. Evidently, the static and dynamic behaviors of marine risers can be simulated considerably well using this theory [4,22]. Morison's equation was used to calculate the hydrostatic and hydrodynamic loads acting on the riser. The finite element method was employed to discretize the governing equations. The static responses were evaluated using numerical integration based on the Newton−Raphson method with iteration. The sensitivity of the riser configuration, effective tension and bending moment to the structural parameters (i.e., buoyancy modules and weight segment) and external loading (i.e., external current and vessel offset) are discussed to broaden the understanding of CVARs.

2. Mathematical model and numerical method

2.1. Slender rod theory

The riser configuration is described by the position of the rod centerline $\boldsymbol{r}(s,t)$, as shown in Fig. 2. Accordingly, the buoyancy modules of the functional segments are approximated as a single riser with equivalent axial and flexural stiffness for a convenient simulation. Based on the conservation of linear momentum, the equation of motion rod can be expressed as follows.

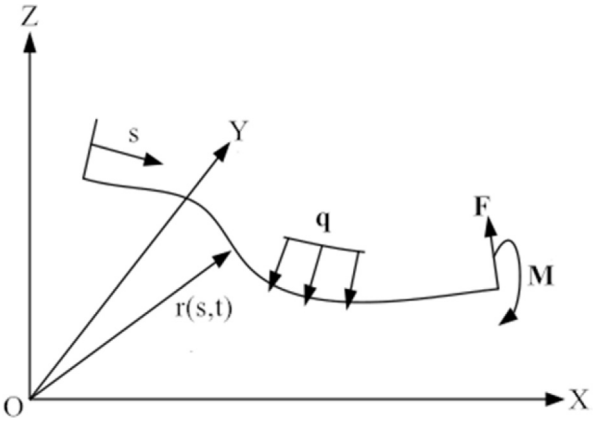

Fig. 2. Diagram of slender rod coordinate [9].

$$-\left(EI\mathbf{r}''\right)'' + (\lambda\mathbf{r}')' + \mathbf{q} = \left(\rho_r + m_f\right)\ddot{\mathbf{r}} \tag{1}$$

where, EI denotes the bending stiffness; $\lambda = T - EI\kappa^2$, T represents the wall tension of rod; ρ_r indicates the mass per unit length; m_f corresponds to the inflow mass per unit length; $\mathbf{q}$ signifies the applied force on the riser's per unit length, which can be given as follows:

$$\mathbf{q} = \mathbf{w} + \mathbf{F}^{\mathbf{s}} + \mathbf{F}^{\mathbf{d}} \tag{2}$$

where, $\mathbf{w}$ denotes the gravitational force, $\mathbf{F}^{\mathbf{s}}$ denotes the hydrostatic force, and $\mathbf{F}^{\mathbf{d}}$ indicates the hydrodynamic force. Accordingly, $\mathbf{F}^{\mathbf{s}}$ can be expressed as follows:

$$\mathbf{F}^{\mathbf{s}} = \mathbf{B} + \left(P_{res}\mathbf{r}'\right)' \tag{3}$$

where, $\mathbf{B}$ denotes the buoyancy force per unit length of the riser, and P_{res} denotes the pressure difference between the inside and outside of the tube. Moreover, the effect of the internal flow is identified and quantified by the plug flow term [3], and the force induced by the internal flow on the riser can be written as follows:

$$f(s,t) = -m_f\left(\frac{\partial^2\mathbf{r}}{\partial t^2} + 2v\frac{\partial^2\mathbf{r}}{\partial s\partial t} + v^2\frac{\partial^2\mathbf{r}}{\partial s^2}\right) \tag{4}$$

where the first, second, and third terms are the inertial force, Coriolis, and centrifugal forces, respectively, whereas v signifies the inflow velocity.

Finally, by substituting Eqs. (2)−(4) into Eq. (1), the riser's governing equation can be obtained as:

$$\left(\rho_r + m_f\right)\ddot{\mathbf{r}} + C_A\ddot{\mathbf{r}}_{\mathrm{n}} + 2m_f v\dot{\mathbf{r}} + \left(EI\mathbf{r}''\right)'' - \left(\overline{\lambda}\mathbf{r}'\right)' = \overline{\mathbf{w}} \tag{5}$$

where $C_A = C_a\rho_w\frac{\pi D^2}{4}$, $\overline{\lambda} = T + P_{res} - EI\kappa^2 = T_e - EI\kappa^2$, $T_e = T + p_oA_o - p_iA_i$, and $\overline{\mathbf{w}} = \mathbf{w} + \mathbf{B}$ denote effective gravity. $\ddot{\mathbf{r}}_{\mathrm{n}}$ indicates the normal acceleration of a rod. The corresponding elongation formula can be expressed by considering that the rod is extensible with linear and small stretches as follows:

$$\frac{1}{2}\left(\mathbf{r}' \cdot \mathbf{r}' - 1\right) - \frac{\overline{\lambda} - p_0A_0 + p_iA_i + m_fv^2}{EA} = 0 \tag{6}$$

where p_i and p_0 denote the pressures inside and outside the riser, respectively, and A_i and A_0 represent the area inside and outside the riser, respectively.

2.2. Finite element discretization

A finite element method (FEM) was used to discretize the entire slender structure into a set of collocation nodes. The physical variables were interpolated according on the nodal values and the shape function with the elements [5].

The governing equation and deformation condition can be written in the tensor form as follows:

$$-\left(\rho + m_f\right)\ddot{r}_i - C_A\ddot{r}_i^n - 2m_fvr_i' - \left(EIr_i''\right)'' + \left(\overline{\lambda}r_i'\right)' + \overline{w}_i = 0 \tag{7}$$

$$\frac{1}{2}\left(r_n'r_n' - 1\right) - \frac{\overline{\lambda} - p_0A_0 + p_iA_i + m_fv^2}{EA} = 0 \tag{8}$$

The variables $r_i(s,t)$ and $\overline{\lambda}(s,t)$ inside each element can be approximately expressed as follows:

$$r_i(s,t) = \sum_{l=1}^{4} A_l(s)U_{il}(t) \tag{9}$$

$$\overline{\lambda}(s,t) = \sum_{m}^{3} P_m(s)\overline{\lambda}_m(t) \tag{10}$$

where, $A_l(s)$ and $P_m(s)$ represent the cubic and quadratic Hermite functions respectively, $l = 1,2,3,4$, $m = 1,2,3$, $0 \le s \le L$; $U_{il}(t)$ denote the vectors of position and tangent, $\overline{\lambda}_m(t)$ represent the vectors of effective tension. Accordingly, the expressions for $A_l(s)$ and $P_m(s)$ are as follows:

$$\begin{aligned} A_1(s) &= 1 - 3\times(s/L)^2 + 2\times(s/L)^3 \\ A_2(s) &= L\left[(s/L) - 2\times(s/L)^2 + (s/L)^3\right] \\ A_3(s) &= 3\times(s/L)^2 - 2\times(s/L)^3 \\ A_4(s) &= L\left[-(s/L)^2 + (s/L)^3)\right] \end{aligned} \tag{11}$$

$$\begin{aligned} P_1(s) &= 1 - 3\times(s/L) + 2\times(s/L)^2 \\ P_2(s) &= 4\times(s/L)[1 - (s/L)] \\ P_3(s) &= (s/L)[2(s/L) - 1] \end{aligned} \tag{12}$$

The final equations can be given as follows:

$$\left(M_{ijlk}+M^{a}_{ijlk}\right)\ddot{U}_{jk}+C^{f}_{ijlk}\dot{U}_{jk}+\left(K^{1}_{ijlk}+\overline{\lambda}_{n}K^{2}_{nijlk}\right)U_{jk}-F_{il}=0 \tag{13}$$

$$G_{m}=A_{mil}U_{ki}U_{kl}-B_{m}+C_{mn}(h_{n}-\overline{\lambda}_{n})=0 \tag{14}$$

where, $M_{ijlk}=\int_0^L(\rho+m_f)A_lA_k\delta_{ij}ds$, $K^1_{ijlk}=\int_0^L EIA''_lA''_k\delta_{ij}ds$, $K^2_{nijlk}=\int_0^L P_nA'_lA'_k\delta_{ij}ds$, $M^a_{ijlk}=C_A[\int_0^L A_lA_k\delta_{ij}ds-(\int_0^L A_lA_kA'_sA'_tds)U_{it}U_{js}]$, $h_n=A_oP_{on}-A_iP_{in}-m_{fn}v^2$, $\delta=\begin{cases}1, & i=j\\ 0, & i=j'\end{cases}$

$C_{mn}=\frac{1}{EA}\int_0^L P_mP_nds$, $C^f_{ijlk}=\int_0^L 2m_fvA'_lA_k\delta_{ij}ds$. The variables i and j are 1, 2, and 3 for the 3-D scenario, the subscripts of l, k, s, and t are 1, 2, 3, and 4, respectively; and m and n are 1, 2, and 3, respectively.

2.3. Static solutions

For the static case, the inertial force was excluded. Hence, the governing equation can be modified as follows:

$$R_{il}=\left(K^{1}_{ijlk}+\lambda_{n}K^{2}_{njilk}\right)U_{jk}-F_{il}=0 \tag{15}$$

$$G_{m}=A_{mil}U_{ki}U_{kl}-B_{m}+C_{mn}(h_{n}-\overline{\lambda}_{n})=0 \tag{16}$$

To perform the static response analysis, the Newton–Raphson method was used to solve the FEM equations in the following manner:

$$R^{(n+1)}_{il}=R^{(n)}_{il}+\frac{\partial R_{il}}{\partial U_{jk}}(\Delta U_{jk})+\frac{\partial R_{il}}{\partial \lambda_{n}}(\Delta\lambda_{n})=0 \tag{17}$$

$$G^{(n+1)}_{m}=G^{(n)}_{m}+\frac{\partial G_{m}}{\partial U_{jk}}(\Delta U_{jk})+\frac{\partial G_{m}}{\partial \lambda_{n}}(\Delta\lambda_{n})=0 \tag{18}$$

Subsequently, the matrix forms of Eqs. (16) and (17) can be obtained as follows:

$$\begin{bmatrix}K^{t0(n)}_{ijlk} & K^{t1(n)}_{i\,\ln}\\ D^{t0(n)}_{mjk}+D^{t0(n)}_{mn} & D^{t1(n)}_{mn}\end{bmatrix}\begin{Bmatrix}\Delta U_{jk}\\ \Delta\lambda_{n}\end{Bmatrix}=\begin{Bmatrix}-R^{(n)}_{il}\\ -G^{(n)}_{m}\end{Bmatrix} \tag{19}$$

$K^{t0(n)}_{ijlk}=K^1_{ijlk}+\lambda^{(n)}_nK^2_{ijlk}$, $K^{t1(n)}_{i1n}=K^2_{nijlk}U^{(n)}_{jk}=(\int_0^L P_nA'_lA'_k\delta_{ij}ds)D^{t1(n)}_{mn}=-\frac{1}{EA}\int_0^L P_nP_mds, D^{t0(n)}_{mjk}=(\int_0^L P_nA'_kA'_pds)U^{(n)}_{jp}, h_n=A_oP_{on}-A_iP_{in}-m_fv^2$,

$D^{t0(n)}_{mn}=\frac{\partial C_{mn}h_n}{\partial U_{jk}}=\frac{\partial}{\partial U_{jk}}C_{mn}(A_oP_{on}-A_iP_{in}-m_fv^2)$,

$R^{(n)}_{ij}=(K^1_{ijlk}+\lambda_nK^2_{ijlk})U^{(n)}_{jk}-F_{il}$,

$G^{(n)}_m=A_{mil}U^{(n)}_{ki}U^{(n)}_{kl}-B_m+C_{mn}(h_n-\lambda^{(n)}_n)$.

The static responses of the CVAR were calculated using MATLAB (R2019b).

3. Model validation

The static response of a steep wave riser was predicted based on the slender rod theory and then compared with Orcaflex to check the applicability of the proposed model. The detailed parameters of this riser were described by [12] and are listed in Table 1. Fig. 3 presents comparisons of the static configuration, bending moment, and effective tension between both methods. It can be observed that the curves given by the model and Orcaflex conform with each other, which demonstrates the feasibility and accuracy of the present theory in resolving the static behavior of marine risers.

4. Results and discussion

Numerous analyses were performed to investigate the static response of the CVAR. The main objective is to investigate the influence of the buoyancy modules and weight segment. Accordingly, the effect of the weight per unit length and length for the functional segments are studied comparatively, with the wet weight remaining unchanged. Additionally, the effects of ocean current and vessel offset on the static behavior of the CVAR are also considered. The CVAR parameters are listed in Table 2.

4.1. The effect of structural parameters

The effect of the initial positions of the buoyancy module were demonstrated by [13]; therefore, that discussion is excluded in this subsection. A first-order factor involving the ratio of wet weight per unit length of the functional segment and bare riser

Table 1. Physical properties of the steep wave riser.

Properties	Value	Properties	Value
Horizontal distance (m)	1200	Outer diameter of the bare riser (m)	0.35
Water depth (m)	1200	Outer diameter of the buoyancy (m)	0.85
Upper region length (m)	1300	Inner diameter of the riser (m)	0.30
Buoyancy region length (m)	600	Axial stiffness (N)	5.0e9
Lower region length (m)	300	Bending stiffness (N·m^2)	6.3e7
Internal fluid density (kg/m^3)	900	Riser material density (kg/m^3)	7850

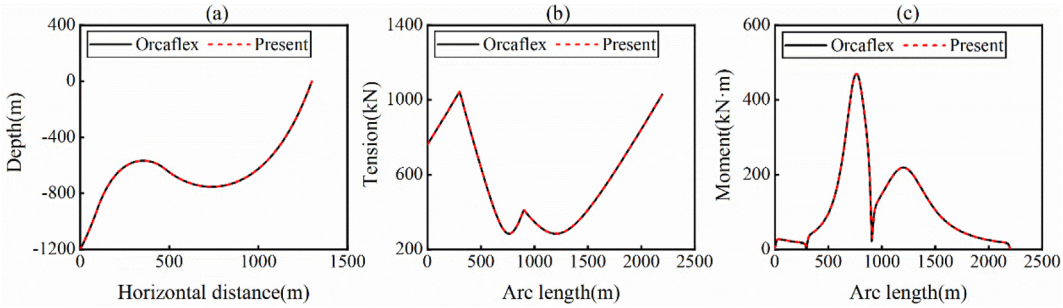

Fig. 3. Comparisons of static response. (a) Configuration; (b) effective tension; (c) bending moment.

Table 2. Physical properties of the CVAR for the basic case.

Properties	Symbol	Value	Properties	Symbol	Value
Horizontal distance (m)	x_L	585	Current velocity (m/s)	V_c	0
Water depth (m)	y_H	2435	Lower region length (m)	L_l	310
Outer diameter of the riser (m)	D	0.35	Buoyancy length in lower part (m)	L_{lb}	190
Axial stiffness (N)	EA	5.36e9	Buoyancy factor in lower part	C_{fl}	5
Bending stiffness (N·m^2)	EI	7.12e7	Transition region length (m)	L_{lt}	420
Riser material density (kg/m^3)	ρ_r	7850	Transition buoyancy factor	C_{ft}	1.6
Internal fluid density (kg/m^3)	ρ_i	900	Gravity length (m)	L_{lg}	100
Internal fluid velocity (m/s)	v	0	Gravity factor	C_{fg}	−1.5
Offset distances along the y-direction (m)	y_L	0	Upper region length (m)	L_u	1780

was introduced to evaluate the additional force effect:

$$C_f = -W_f/W \tag{20}$$

where, W_f signifies the wet weight per unit length of the functional modules and W denotes the wet weight per unit length of the bare riser.

4.1.1. Sensitive to buoyancy module in lower region

The objective of the buoyancy module in the lower region is to maintain the vertical state of the bottom parts, which determines the operational advantage. The effects of the length and factors of this buoyancy module are investigated in detail.

Fig. 4 presents the configuration, bending moment, and effective tension along the CVAR for four different lengths of the buoyancy module. Evidently, it can be observed that the overall static configuration almost coincides in four cases, and the bending moment distribution exhibits little variation. Only the bending moment extremum near the bottom end changes position, and there is a phenomenon where its variation value is the same as that of the buoyancy segment's length. Accordingly, the effective tension in the bottom end grows significantly following the increase of the buoyancy force. The above results indicate that the length of the buoyancy module primarily has an effect on the static response of the lower region, particularly for the bottom tension, whereas it hardly influences the transition and upper regions. Fig. 5 presents the effect of buoyancy factor on the mechanical properties of the CVAR. Accordingly, the lower and

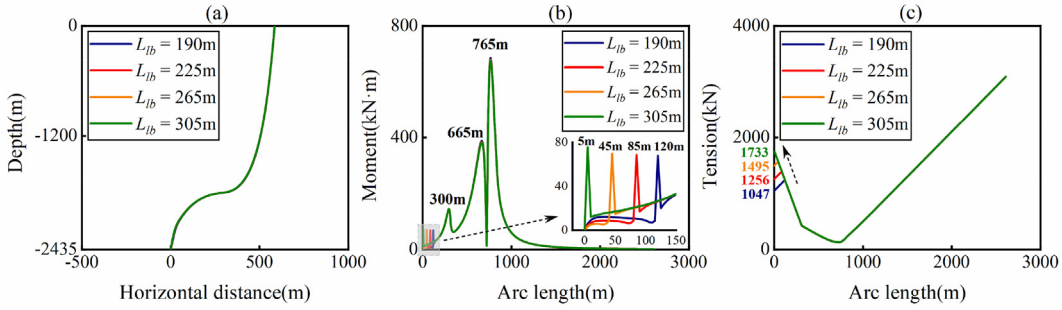

Fig. 4. Static responses of the CVAR with different lengths of the buoyancy module. (a) configuration. (b) bending moment. (c) effective tension.

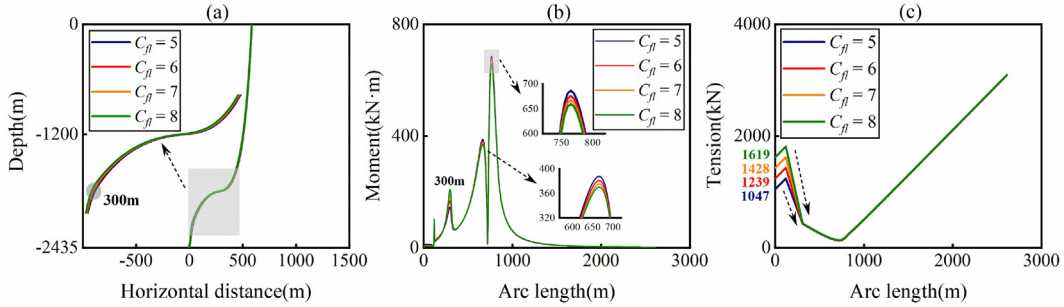

Fig. 5. Static responses of the CVAR with different factors of the buoyancy module. (a) configuration. (b) bending moment. (c) effective tension.

transition regions move along the -x direction slightly with increasing buoyancy factors. The bending point between both regions is more obvious, which leads to an increment in the bending moment at 300 m. However, the opposite is true for the bending moment at the arch and sag bend. It is primarily because the radius of curvature decreases at both bend points due to variation of configuration. As expected, the bottom tension increases remarkably. Moreover, the slope in effective tension of the buoyancy module also varies. Evidently, Fig. 4 and Fig. 5 show that the bottom tension is more sensitive to the length of the buoyancy module due to the shortening in the length of the bare riser. Hence, the bottom end sustains a relatively low-level tension by adjusting the buoyancy factor, although the extremum of bending moment increases slightly.

4.1.2. Sensitive to buoyancy module in transition region

The buoyancy segment in the transition region is one of the determining factors for the CVAR configuration and plays a critical role in isolating movement from the top end. The influence of the buoyancy module length and factor on the static response is analyzed.

Fig. 6 depicts the influence of the buoyancy module's length on the configuration, bending moment and effective tension along the CVAR. The configuration appears as the approximate horizontal segment uplifts with increasing buoyancy force. Consequently, the bending moment of arch and sag bend increases, moving their locations in the distance same as the variation of length. However, the trend of the bending moment at 300 m is opposite, and the reason is that the riser part close to this point becomes more compliant. Meanwhile, the bottom tension increases with increasing the buoyancy lengths, whereas a decreasing trend occurs in the top tension. It is primarily because the reduced gravity of the upper region (108 kN, 98 kN, 98 kN) results in the decline of the top tension (98 kN, 84 kN, and 84 kN). Therefore, it can be concluded that the length of the buoyancy module has a relatively significant influence on the lower and transition regions. The effects of buoyancy factors on the mechanical behaviors of the CVAR are illustrated in Fig. 7. Accordingly, most regions vary slightly as the buoyancy force per unit length increases. The bending moment at the arch bend increases significantly; however, it grows slightly at the sag bend. The result can be explained that the arch bend section is primarily composed of a buoyancy module, and it is easily affected by the variation of buoyancy force. Additionally, the bending moment at 300 m decreases, and the reason is the same as the mentioned above from Fig. 6. An increment in the

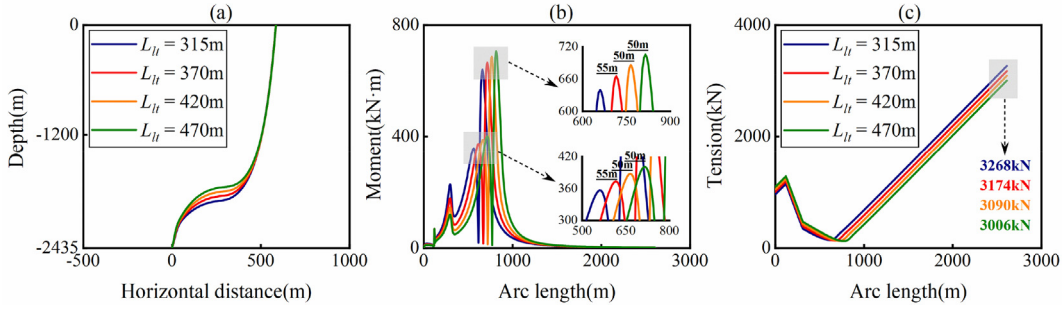

Fig. 6. Static responses of the CVAR with different lengths of the buoyancy module. (a) Configuration; (b) bending moment; (c) effective tension.

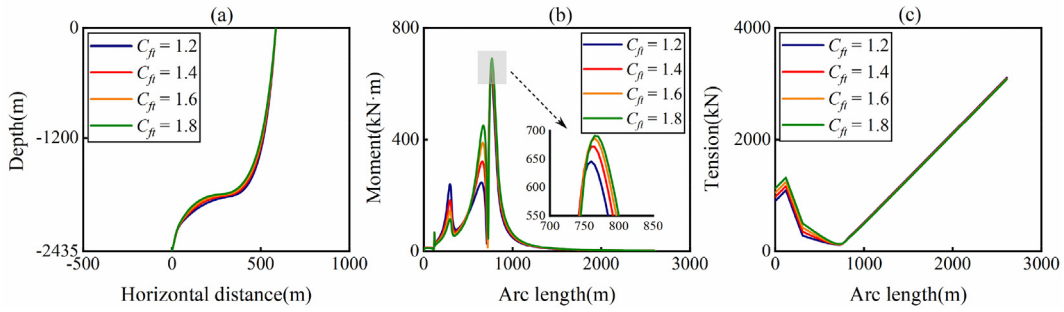

Fig. 7. Static responses of the CVAR with different factors of the buoyancy module. (a) Configuration. (b) bending moment. (c) effective tension.

buoyancy factor only increases the effective tension of the lower region, while the top tension remains almost constant. Therefore, the increment of the buoyancy force per unit length hardly influences the top tension. The conclusion can be obtained from the comparison that an appropriate increase in the buoyancy module's length can reduce the top tension, and the situation that the bending moment extremums grows significantly can also be avoided as much as possible.

4.1.3. Sensitive to the weight segment

The weight segment is a critical component in the realization of a special CVAR configuration, which primarily contributes to the vertical state of the top end. A static analysis of the effect of this segment is carried out in this subsection.

Fig. 8 illustrates the effect of the weight segment length on the static response of the CVAR. It can be observed that there is little variation in the configuration as the length increases, and the bending moment at arch and sag bend points increase slightly. Meanwhile, the effective tension increases only in the upper region. Besides, the increments of top tension are 34 kN, 37 kN, and 34 kN respectively, which almost coincide with the wet weight increment of the weight segment (32 kN, 34 kN, and 32 kN). It indicates that the wet weight of the weight segment acts entirely on the top tension. Fig. 9 illustrates the effect of the weight segment factor on the static response of the CVAR. As the weight factor increases, the configuration near the weight segment descends, which leads to a sharp reduction of curvature radius at the sag bend. Consequently, its bending moment increases remarkably, and an obvious inflection point was also found. However, the bending moment of arch bend varies little. In other words, the weight segment primarily influences the sag bend. The effective tension distribution demonstrates that the weight factor also has a significant effect on the effective tension of the upper region. Additionally, the same phenomenon also appears that the increment of wet weight (101 kN, 100 kN, and 100 kN) is almost equal to that of top tension (97 kN, 100 kN, and 101 kN). It can be obtained from the comparison between both figures that the factor of weight segment has a more significant impact on the static response of CVAR. Thus, it is important to pay attention to the factor of weight segment in the design process, which, in turn, prevents an excessive bending moment extremum value.

4.2. The effect of external loads

Four load cases with different ocean current velocities (−0.5 m/s, −0.25 m/s, 0.25 m/s, and 0.5 m/s) and vessel offset distances (−120 m, −60 m, 60 m,

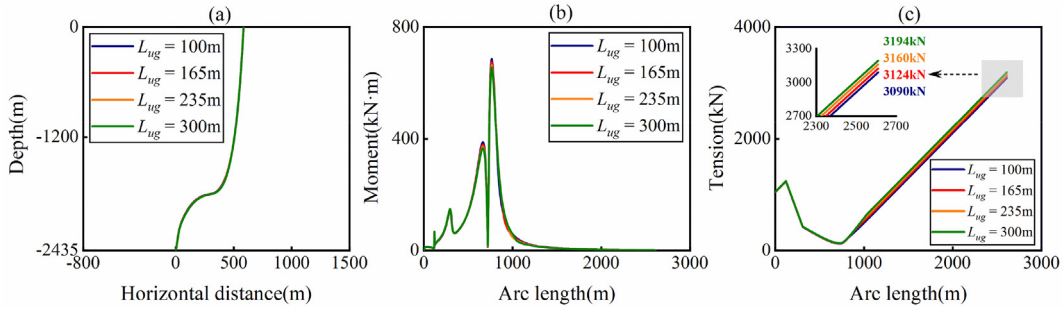

Fig. 8. Static responses of the CVAR with different lengths of the weight segment. (a) Configuration. (b) bending moment. (c) effective tension.

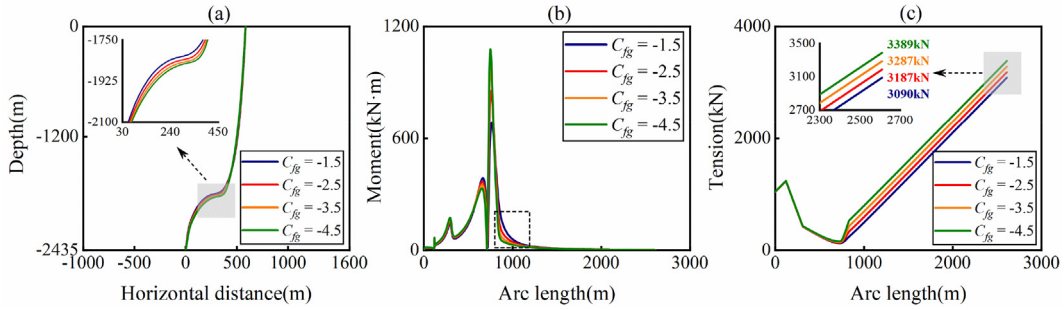

Fig. 9. Static responses of the CVAR with different factors of the weight segment. (a) Configuration; (b) bending moment; (c) effective tension.

and 120 m) were arranged to investigate the effects of ocean current and vessel offset on the mechanical behavior of the CVAR. A negative value indicates an opposite direction.

4.2.1. The effect of current

Fig. 10 depicts the static response under current along the x-direction. Accordingly, when the current velocity varies from -x to + x direction, the riser configuration moves along the x-axis appreciably, and the maximum displacements are 28.27 m, 6.89 m, 6.77 m and 26.33 m, respectively. The horizontal segment moves down, which can be explained as the current in the negative direction, the drag force on the riser has an upward component, whereas it is opposite to the positive current. There is a significant change of bending moment in the sections of arch bend and sag bend. The effective tension distribution changes slightly with the varying current due to the relatively small drag force. Moreover, the results were also obtained by the static behavior is not symmetric around $V_c = 0$. The coupled effect of the hydrodynamic loads with the axial tension is the primary reason for this phenomenon [24].

Fig. 11 illustrates the effects of the current along the y-direction on the static response of the CVAR. It can be observed that the configuration is symmetric under the flow velocity in different directions with equal value and the maximum displacements are 11.72 m and 46.52 m. Moreover, it was found that the current in the y direction has no effect on the displacement along the x-direction, primarily because the projection of the CVAR onto the xz plane varies slightly. The bending moment extremum decreases slightly as the current velocity increases, and the effective tension is almost unchanged. Therefore, the results mean that the current y-direction has a weak influence on the mechanical performance of the CVAR.

By contrasting Fig. 10 and Fig. 11, the results reveal that the deformation induced along y-direction is larger, which is due to the orthogonal relationship between the current direction and riser. However, the effect of the current along the x-direction current on the mechanical performance was more significant than that in the y-direction. Likewise, it can be observed that the static behavior changes moderately when the current velocity is relatively low; however, it changes dramatically with an increase in the current velocity. Therefore, the high current velocity should be considered during the design stage.

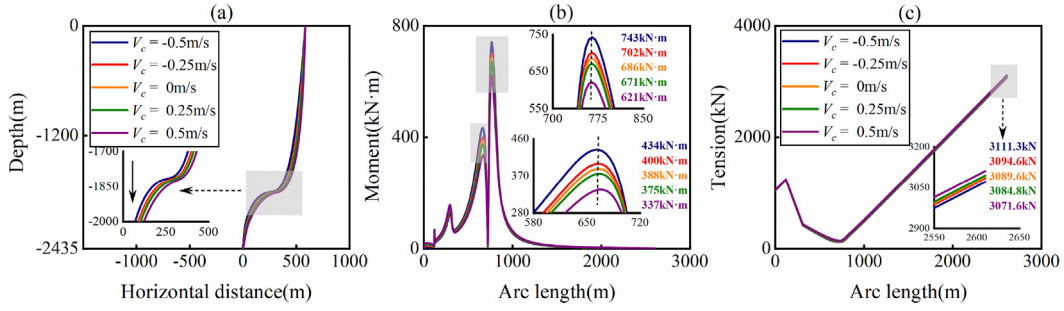

Fig. 10. Static responses of the CVAR under different current velocities along the x-direction. (a) Configuration; (b) bending moment; (c) effective tension.

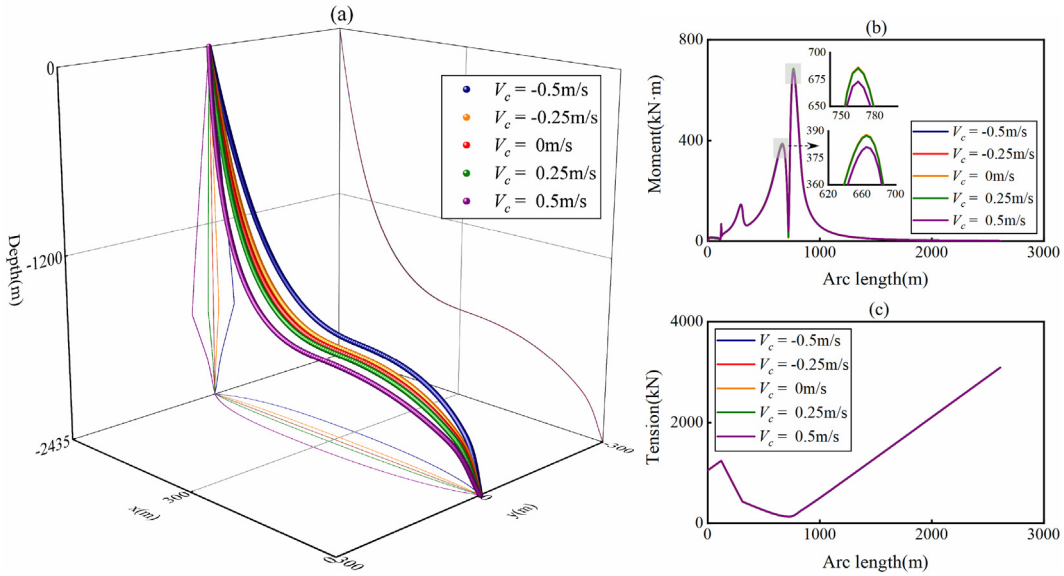

Fig. 11. Static responses of the CVAR under different current velocities along the y-direction. (a) Configuration; (b) bending moment; (c) effective tension.

4.2.2. The effect of vessel offset

The static responses of the CVAR for different offset distances along the y-direction are presented in Fig. 12. It can be observed that as the offset distance varies from the -x to + x direction, the configuration changes significantly, particularly for arch and sag bends. The bending moment at both bend points decreases dramatically. The effective tension clearly increases, and it also demonstrates that the farther the vessel is located, the more the top tension will grow. Accordingly, Fig. 13 reveals that only the offset distance has a certain effect on the static response of the CVAR owing to the symmetry. The bending moment at both bend points decreases slightly with increasing offset distance, and the effective tension distribution remains nearly constant. Therefore, the results indicate that the drift in the y-direction has a weak influence on CVAR, although there is a difference in the bending moments curves. We can conclude from Fig. 12 and Fig. 13 that under the same offset distance, the effect of the drift in the x-direction is more notable, particularly the variation in bending moment. It is essential to note that both ends of the CVAR may lose their vertical state as the offset increases markedly along the +x or y direction. Thus, maintaining a suitable offset distance is key to the safe operation of CVAR.

5. Conclusion

The static response of the CVAR was conducted in this study with the effects of structural parameters and external loads using the slender rod theory. The internal flow was incorporated into all segments of the CVAR. The key conclusions are drawn in the following paragraphs by analyzing the numerical simulation results.

(1) The buoyancy parameters of the lower region primarily influence the effective tension distributions in the bottom parts, and the effect of the

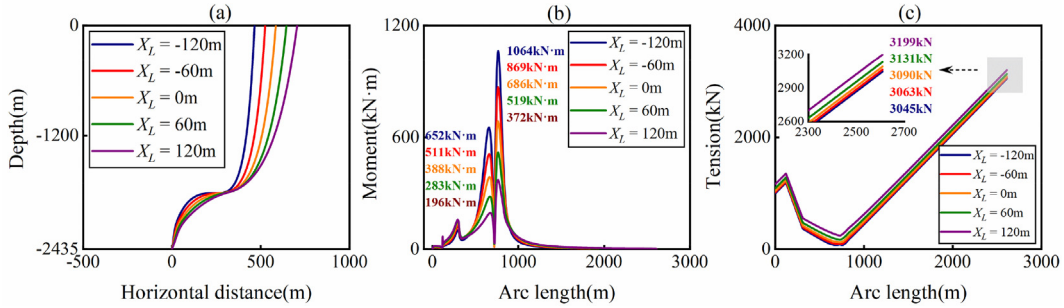

Fig. 12. Static responses of the CVAR under different offset distances along the x-direction. (a) Configuration; (b) bending moment; (c) effective tension.

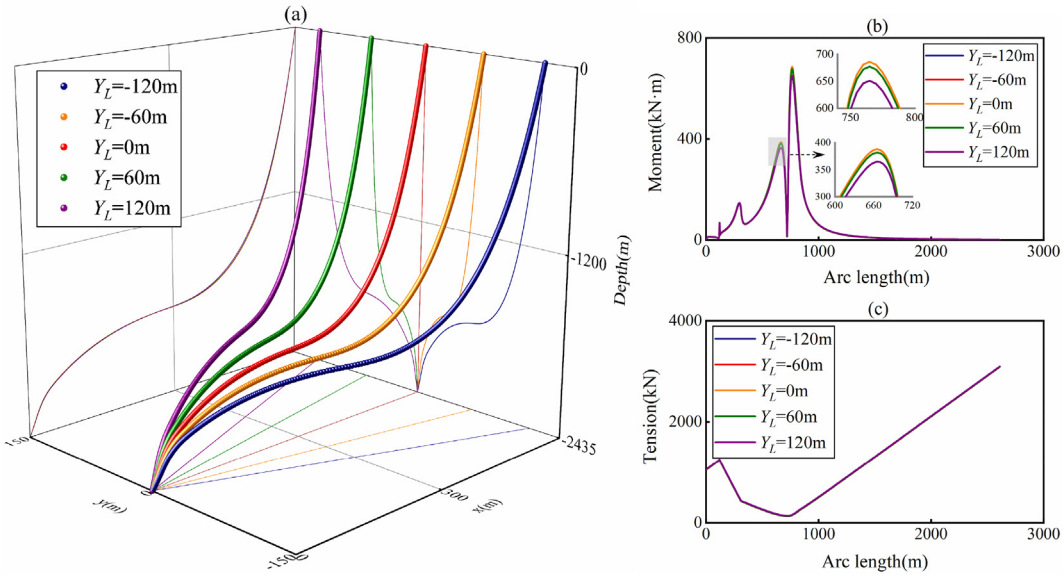

Fig. 13. Static responses of the CVAR under different offset distances along y-direction. (a) Configuration; (b) bending moment; (c) effective tension.

length is more significant owing to the decrease in the length of the bare riser. In addition, the variation rate of the lower region's tension is the primary difference between the two parameters in the static response of the CVAR.

(2) With increasing buoyancy force in the transition region, the horizontal segment uplifts, the bending moments in the arch and sag bend increase, and the bottom tension also increases. However, the opposite is true for the bending moment at the position of 300 m because the increased buoyancy leads to a more compliant riser segment near the point. Compared with the buoyancy factor, an increase in the length changes the position of the bending moment extremum and also leads to a decrease in the effective tension at the top because of the decrease in the upper region.

(3) The effect of the weight segment length within a certain range on the overall mechanical properties of CVAR is weak. The factor of this module had a relatively significant influence on the bending moment extremum and top tension. Thus, it is important to avoid a high factor for the weight segment. Additionally, an increase in the wet weight of the weight segment occurs almost entirely on the top tension.

(4) The static responses of the CVAR are susceptible to the current along the x-direction, particularly for the bending moment at the arch and sag bend segments. The current velocity along the y-direction had a significant influence only on the displacement in the same direction. The static behavior changes moderately when the current velocity is relatively low; however, it increases dramatically with the increasing x- and y-current velocities.

(5) The vessel offset in the x-direction has a more prominent influence on the static response of the CVAR than that in the y-direction, particularly for the bending moment at the archand sag bend parts. The most significant issue induced by the floating body drift is that the CVAR loses its vertical state at the bottom under a larger offset.

In summary, this study is intended to enhance the understanding of structural parameters and marine loadings. It is crucial to pay attention to these factors during the design process. In the future, we intend to further investigate the dynamic response [7,8,10,20,26].

Conflicts of interest

There is no conflict of interest.

Acknowledgements

This work was supported by National Natural Science Foundation of China (U2006226, 51979257), and Shandong Provincial Natural Science Foundation, China (ZR2020ME261, ZR2019MEE032).

References

[1] Brinkmann CR, Whooley KT. Design study of a deepwater compliant vertical access riser for the Gulf of Mexico. In: Proceedings of the ASME 21st international conference, offshore mechanics and arctic engineering; 2002.

[2] Claudio MSD, Marcos QDS, Ellwanger GB, Analúcia FLT, Marcio MM. A frequency domain approach for random fatigue analysis of steel catenary risers at Brazil's deepwaters. In: ASME 23rd International Conference; 2004.
[3] Chen X. Studies on dynamic interaction between deep-water floating structures and their mooring/tendon systems. Doctoral thesis. Texas A&M University; 2002.
[4] Cheng Y, Tang LY, Fan TH. Dynamic analysis of deepwater steel lazy wave riser with internal flow and seabed interaction using a nonlinear finite element method. Ocean Eng 2020;209:107498.
[5] Cheng Y, Ji C, Zhai G, Oleg G. Nonlinear analysis for ship-generated waves interaction with mooring line/riser systems. Mar Struct 2018;59:1−24.
[6] Chris M, Kevin H, Shankar B, David A, Indranil S, Jack W, et al. Semisubmersible based dry tree platform with compliant vertical access risers. Houston, Texas: Offshore Technology Conference; 2004. p. 1−13.
[7] DNV. Dynamic risers. Det Norske Veritas, Offshore standard DNV-OS-F201. 2010.
[8] Fan TH, Ren NX, Cheng Y, Chen CH, Ou JP. Applicability analysis of truncated mooring system based on static and damping equivalence. Ocean Eng 2018;147:458−75.
[9] Garrett DL. Dynamic analysis of slender rods. J Energy Resour Technol 1982;104:302−6.
[10] Kuroiwa T, Nishigaki M. Interaction between riser and tubing in CVAR system. In: Proceedings of the twelfth international offshore and polar engineering conference. Havaii; 2002. p. 26−31.
[11] Lenci s, Callegari M. Simple analytical models for the J-lay problem. Acta Mech 2005;178:23−39.
[12] Liu Z, Guo HY. Sensitivity analysis of steep wave riser with internal flow. J Mar Sci Technol 2018;26(4):541−51.
[13] Lou M, Li R, Wu WG, Chen ZS. Static performance analysis of deepwater compliant vertical access risers. Int J Naval Archit Ocean Eng 2019a;11(2):970−9.
[14] Lou M, Zhang Y, Wu WG. Static optimization of a compliant vertical access riser. J Ocean Univ China 2019b;18(5):1070−8.
[15] Lou M, Liang WX, Li R. Experimental and numerical study of dynamic performance of CVAR subjected to regular wave and platform motion. Ocean Eng 2020;199:106946.
[16] Martins MAL, Silveira ESS. Statistical design of experiments applied to the design of compliant vertical access risers. ASME 31st International Conference on Ocean, Offshore Arctic Engineering. 2012.
[17] Martins MAL, Lages EN, Silveira SS. Compliant vertical access riser assessment: DOE analysis and dynamic response optimization. Appl Ocean Res 2013;4:28−40.
[18] Paulling JR, Webster WC. A consistent large amplitude analysis of the coupled response of a TLP and Tendon System. Japan: Proceedings of the 5th OMAE Symposium; 1986. p. 126−33.
[19] Pearce JL, Sizer PS, Gano JC, Yonker JH, Thurman RL, O'Sullivan JF, et al. Method and system for maintenance and servicing of subsea wells, United States Patent No. 4730677. 1988.
[20] Romero I. A comparison of finite elements for nonlinear beams: the absolute nodal coordinate and geometrically exact formulations. Multibody Syst Dyn 2008;20(1):51−68.
[21] Ruan WD, Shang ZH, Wu JG. Effective static stress range estimation for deepwater steel lazy-wave riser with vessel slow drift motion. Ships Offshore Struct 2019;14(8):899−909.
[22] Ruan WD, Dai W, Wu JG. Study on motion transfer rule and extreme dynamic response of SCR's top-end heave excitation. J Mar Eng Technol 2019:1−14.
[23] Tan RL, Duan ML, Wang ZM, Ning H. Numerical calculation model investigation on response for connector assembly of a free-standing hybrid riser with experimental validation. Ocean Eng 2018;155:144−55.
[24] Trapper PA. Feasible numerical analysis of steel lazy-wave riser. Ocean Eng 2020;195:106643.
[25] Wang JL, Duan ML. A nonlinear model for deepwater steel lazy wave riser configuration with ocean current and internal flow. Ocean Eng 2015;94:155−62.
[26] Wang JL, Duan ML, He RY. A nonlinear dynamic model for 2D deepwater steel lazy-wave riser subjected to top-end imposed excitations. Ships Offshore Struct 2018;13(3):330−42.
[27] Zhen WQ, Yang HZ. Dynamic response optimization of a compliant vertical access riser. Ship Sci Technol 2010;32(2):114−9.